JOURNAL OF MATERIALS RESEARCH AND TECHNOLOGY 2021;13:2336–2349

Available online at www.sciencedirect.com

jmr&t Journal of Materials Research and Technology

journal homepage: www.elsevier.com/locate/jmrt

Original Article

Cadmium oxide reinforced $46V_2O_5$–$46P_2O_5$–(8–x) B_2O_3–xCdO semiconducting oxide glasses and resistance behaviors against ionizing gamma rays

H.O. Tekin [a,b], Shams A.M. Issa [c,d], G. Kilic [e], Hesham M.H. Zakaly [c,f,*], A. Badawi [g,i,***], G. Bilal [a], H.A.A. Sidek [h], K.A. Matori [h], M.H.M. Zaid [h,**]

[a] Medical Diagnostic Imaging Department, College of Health Sciences, University of Sharjah, Sharjah, 27272, United Arab Emirates
[b] Medical Radiation Research Center (USMERA), Uskudar University, Istanbul, 34672, Turkey
[c] Physics Department, Faculty of Science, Al-Azhar University, Assiut, 71524, Egypt
[d] Physics Department, Faculty of Science, University of Tabuk, Tabuk, 71451, Saudi Arabia
[e] Department of Physics, Eskisehir Osmangazi University, Eskisehir, 26040, Turkey
[f] Institute of Physics and Technology, Ural Federal University, Ekaterinburg, 620000, Russia
[g] Department of Physics, College of Science, Taif University, P.O. Box 11099, Taif, 21944, Saudi Arabia
[h] Department of Physics, University Putra Malaysia, Serdang, 43400, Selangor, Malaysia
[i] Department of Physics, University College of Turabah, Taif University, P.O. Box 11099, Taif, 21944, Saudi Arabia

ARTICLE INFO

Article history:
Received 17 January 2021
Accepted 7 June 2021
Available online 12 June 2021

Keywords:
Semiconducting oxide glasses
Shielding
MCNPX
Phy-X PSD
CdO

ABSTRACT

This study aimed to determine the contribution of B_2O_3/CdO substitution on gamma-ray attenuation behaviors of $46V_2O_5$–$46P_2O_5$–(8–x)B_2O_3–xCdO (x = 0–8 mol%) glass system. Accordingly, attenuation coefficients along with half and tenth value layers of five different samples were determined in 0.015 MeV–15 MeV photon energy range. Moreover, effective atomic numbers and effective atomic weight along with exposure and energy absorption buildup factors were determined in same energy range. The result showed that B_2O_3/CdO substitution has a direct effect on behaviors of studied semiconducting oxide glasses against ionizing gamma-rays. Our findings showed that increasing CdO reinforcement has an obvious impact on gamma-ray attenuation properties especially in the low energy range, where photoelectric effect dominates the photon–matter interaction. Moreover, half-value layer, mean-free path and tenth value layer also decrease with an increase in the content of CdO in the composition. Consequently, VPBCd8 sample with 8% mole CdO additive was reported with the minimum half-value layer, the mean-free path, tenth value layer exposure build-up factor and energy absorption build-up factors. The outcomes would be useful for scientific community to observe the most suitable substitution type along with related semiconducting oxide glass composition to provide the aforementioned shielding properties in terms of needs and utilization requirements.

* Corresponding author. Institute of Physics and Technology, Ural Federal University, Ekaterinburg, 620000, Russia.
** Corresponding author.
*** Corresponding author. Physics Department, Faculty of Science, University of Tabuk, Tabuk, 71451, Saudi Arabia.
E-mail addresses: h.m.zakaly@azhar.edu.eg (H.M.H. Zakaly), daraghmeh@tu.edu.sa (A. Badawi), drhafizzaid2020@gmail.com (M.H.M. Zaid).

https://doi.org/10.1016/j.jmrt.2021.06.020

1. Introduction

Along with the more prevalent SiO_2, P_2O_5, and B_2O_3, V_2O_5 is also known as a glass former [1]. However, the literature review showed that B_2O_3 is the most robust glass former among the aforementioned former types [2]. Due to their technical applications and promising optical, physical, mechanical, electrical, and magnetic properties of pure rare-earth, metal-doped alkali/alkaline earth borate glasses with various transitions have recently begun to gather interest from researchers [3–6]. Owing to the fascinating electronic, optical, and magnetic properties of transition metal-doped glasses, several studies are found in the literature, although few studies [7–10] are found in glasses containing high vanadium oxide levels. The glass is semiconducting because it comprises an electrical valence of V^{4+} and V^{5+} [11]. Vanadium doped glasses are a constant concern since they are used in various optical and electrical applications. With a broader range of uses, it has a broader scope of use with fibre optics in the formation of solid-state computers. In contrast to other glass-based substrates, phosphates have an excellent role in mobile system applications owing to their low melting temperatures [12,13]. Owing to the low levels at which they can capture ions, rare-earth ion-doped phosphate glasses are ideal for optical and laser applications. Apart from the industrial areas, utilization of glasses in medical radiation facilities is increasing day-by-day. Some international authorities such as International Atomic Energy Agency (IAEA) and World Health Organization (WHO) have started this trend considering the toxic effects and low material durability of traditional shielding materials such as lead (Pb) and concrete [14,15]. Therefore, researchers were encouraged to evaluate different forms of glass, alloy and composite materials to discover new generation of effective and environmentally sustainable protective materials. Glass products are useful for several factors including simplicity of design, low expense, ease of usage, and optical transparency. In actuality, Pb and Pb-based shielding materials are harmless to biological species [16]. As a result, glass materials with advanced physical properties against ionizing radiation are of considerable interest due to their potential benefits. The amorphous structure of glass is a unique physical state that differs greatly from crystals and other forms of material [17]. There are also different compositions of glassy structures that can be synthesized by using several glass formers and additive materials like transition metals, alkalis, alkaline earths as modifiers [18–20]. On the other hand, glass density is another feature that should always be considered in nuclear radiation shielding competences. In this research, multiple effects of B_2O_3 replacement by CdO were investigated in $46V_2O_5–46P_2O_5–(8\text{-}x)B_2O_3–xCdO$ ($x = 0–8$ mol%) glass system. The main focus of our investigation was to see potential impacts of increasing CdO (from 0 to 8 mol%) additive on nuclear radiation shielding competencies of $46V_2O_5–46P_2O_5–(8\text{-}x)B_2O_3–xCdO$ glass system. Previous study [1] showed that different types of advantageous properties were obtained by B_2O_3/CdO substitution. However, potential consequences of this substitution on radiation attenuation competencies have not been investigated yet. Therefore, we hypothesised that substitution of B_2O_3 with CdO might contribute to gamma-ray attenuation properties of studied glass samples. Consequently, various types of critical parameters were calculated, as shown below.

- Linear attenuation coefficients (LAC)
- Mass attenuation coefficients (MAC)
- Half value layer ($T_{1/2}$)
- Mean free path (λ)
- Tenth value layer (TVL)
- Effective atomic number (Z_{eff})
- Effective electron density (N_{eff})
- Exposure build-up factor (EBF)
- Energy absorption build-up factor (EABF)

The outcomes of recent investigation would be useful for scientific community to understand potential consequences of B_2O_3/CdO substitution on radiation shielding properties of semiconducting oxide glasses.

2. Methods and materials

Simulation studies for gamma-ray transmission: In this study, mass attenuation coefficients (MAC) of $46V_2O_5–46P_2O_5–(8\text{-}x)B_2O_3–xCdO$ ($x = 0–8$ mol%) [1] glass system were determined by using Phy-X PSD [21] code and

Table 1 – Chemical compositions and density for glass samples.

Glass Code	mol%				wt%					Density (g/cm^3)
	V_2O_5	P_2O_5	B_2O_3	CdO	B	O	P	V	Cd	
VPBCd0	46	46	8	0	0.011193	0.501109	0.184408	0.30329	0	2.812
VPBCd2	46	46	6	2	0.008331	0.493215	0.183015	0.301	0.014439	2.854
VPBCd4	46	46	4	4	0.005513	0.485439	0.181644	0.298744	0.028662	2.899
VPBCd6	46	46	2	6	0.002736	0.477778	0.180292	0.296521	0.042672	2.948
VPBCd8	46	46	0	8	0	0.470231	0.178961	0.294331	0.056476	3.011

Table 2 – Mass attenuation coefficients (MAC) of studied glass samples obtained from MCNPX code and Phy-X PSD program.

Energy (MeV)	VPBCd0		VPBCd2		VPBCd4		VPBCd6		VPBCd8	
	Phy-X PSD	MCNPX	Phy-X PSD	MCNPX	Phy-X PSD	MCNPX	Phy-X PSD	MCNPX	Phy-X PSD	MCNPX
0.015	15,3115	15,6354	15,7661	15,8536	16,2379	16,2956	16,7026	16,8236	17,1604	17,2036
0.02	6,7963	6,8124	7,0072	6,9854	7,2255	7,2324	7,4405	7,4521	7,6524	7,6624
0.03	2,1961	2,2021	2,7176	2,7426	3,2347	3,2412	3,7441	3,7523	4,2459	4,2462
0.04	1,0322	1,0526	1,2780	1,2924	1,5216	1,5325	1,7616	1,7752	1,9980	2,0078
0.05	0,6089	0,6124	0,7433	0,7526	0,8766	0,8792	1,0078	1,0109	1,1371	1,1398
0.06	0,4182	0,4209	0,4996	0,5021	0,5803	0,5816	0,6598	0,6621	0,7382	0,7416
0.08	0,2614	0,2632	0,2978	0,3008	0,3339	0,3342	0,3695	0,3716	0,4045	0,4065
0.10	0,2011	0,2036	0,2204	0,2256	0,2396	0,2409	0,2585	0,2591	0,2771	0,2798
0.15	0,1471	0,1483	0,1531	0,1541	0,1590	0,1598	0,1649	0,1651	0,1707	0,1724
0.20	0,1264	0,1271	0,1289	0,1296	0,1315	0,1319	0,1340	0,1344	0,1365	0,1686
0.30	0,1056	0,1060	0,1063	0,1064	0,1070	0,1086	0,1077	0,1089	0,1085	0,1094
0.40	0,0934	0,0942	0,0937	0,0945	0,0939	0,0943	0,0942	0,0945	0,0945	0,0952
0.50	0,0849	0,0852	0,0849	0,0855	0,0851	0,0858	0,0852	0,0860	0,0853	0,0864
0.60	0,0783	0,0789	0,0783	0,0792	0,0783	0,0793	0,0783	0,0795	0,0784	0,0796
0.80	0,0686	0,0691	0,0685	0,0693	0,0685	0,0694	0,0685	0,0696	0,0684	0,0699
1.00	0,0616	0,0621	0,0615	0,0624	0,0615	0,0625	0,0614	0,0627	0,0614	0,0634
1.50	0,0502	0,0511	0,0501	0,0515	0,0500	0,0516	0,0500	0,0519	0,0499	0,0521
2.00	0,0433	0,0436	0,0433	0,0439	0,0433	0,0441	0,0432	0,0445	0,0432	0,0447
3.00	0,0355	0,0357	0,0356	0,0360	0,0356	0,0361	0,0356	0,0364	0,0356	0,0366
4.00	0,0312	0,0315	0,0313	0,0319	0,0314	0,0321	0,0314	0,0323	0,0315	0,0325
5.00	0,0286	0,0291	0,0287	0,0295	0,0288	0,0297	0,0289	0,0298	0,0290	0,0309
6.00	0,0268	0,0273	0,0269	0,0276	0,0271	0,0278	0,0272	0,0279	0,0273	0,0281
8.00	0,0246	0,0248	0,0248	0,0251	0,0250	0,0254	0,0252	0,0256	0,0254	0,0260
10.00	0,0235	0,0237	0,0237	0,0238	0,0240	0,0241	0,0242	0,0244	0,0244	0,0245
15.00	0,0223	0,0225	0,0227	0,0228	0,0230	0,0231	0,0233	0,0236	0,0236	0,0238

MCNPX [22] Monte Carlo code considering their chemical compositions and densities (see Table 1). The obtained MAC values can be obtained from Table 2. Overall, MAC values were obtained in well agreement and in same variation trend. However, slight differences were reported between Phy-X PSD code and MCNPX Monte Carlo code. This can be explained by natures of these two tools that MCNPX uses Monte Carlo method and random event generator in modelled simulation environment, whereas Phy-X PSD is a tool that uses mathematical calculations for direct determination of MAC values. Firstly, MCNPX input data was created considering cell cards, surface cards, and source information. In a Lead (Pb) shield block, an isotropic point source was located. Following that, models of the glass specimens were created using their elemental compositions (percent weight) and material densities (g/cm^3). A cylindrical geometry with a radius of 5 cm was used to form the glass specimen. As a result, cell card boundaries were filled with necessary material properties (i.e. elemental mass fraction and material density). Table 1 summarizes the elemental mass fractions of the studied glasses. It is worth noting that the Mn variable card was used to define the elemental description of glass specimens. Following the initial step of cell description, the value of photon and electron interactions was calculated (i.e. IMP: p, e). This can be demonstrated by the fact that the MCNPX code employs a variance reduction technique. On the other hand, a detection field (F4 Tally Mesh) was located for counting attenuated (secondary) gamma rays. This tally mesh can be used to determine the average photon flux within a point or cell. It is worth mentioning that a Pb block shield was used to protect the detector field in order to absorb scattered gamma rays and increase detection sensitivity. Every run was repeated for 10^8 particles of each glass sample at various photon energies (i.e. from 0.015 MeV to 15 MeV) in the simulation. For all simulations, the uncertainty associated with MCNPX was less than 1%.

Shielding parameters: If the attenuator material as shield is positioned between the detector and the source, intensity of primary gamma-ray decreases exponentially due to Beer–Lambert law [23,24]:

$$I = I_o e^{-\mu x} \tag{1}$$

I_o is the intensity of primary gamma, while I is the intensity of transmitted gamma through the glass. Besides, μ indicates the linear attenuation coefficient of the energy of interest. The term of x is the thickness of attenuator sample. In the case of a compound, the mass attenuation coefficients (MAC) of glasses are estimated [25,26]:

$$MAC = \sum_i w_i (MAC)_i \tag{2}$$

where w_i is the weight fraction of the i^{th} constitute elements.

The effective atomic number and effective electron density, depending on the total molecular cross-section (σ_t), total atomic cross-section (σ_a) and total electronic cross-section (σ_e), was used to measure the total effective atomic cross-section [27,28].

$$\sigma_t = \frac{1}{N_A} \sum_i n_i A_i (MAC)_i \tag{3}$$

$$\sigma_a = \frac{1}{N_A}\sum_i f_i A_i (MAC)_i \quad (4)$$

$$\sigma_e = \frac{1}{N_A}\sum_i \frac{f_i A_i}{Z_i} (MAC)_i \quad (5)$$

$$Z_{eff} = \frac{\sigma_a}{\sigma_e} \quad (6)$$

$$N_{eff} = \frac{(MAC)}{\sigma_e} \quad (7)$$

where n_i, A_i, Z_i, f_i and N_A are the number of atoms, atomic weight, atomic number, fractional abundance of ith element and Avogadro number, respectively. A certain attenuator thickness can decrease the absorbed gamma intensity to 1/2 of the premier radiation: this is called the half-value layer (HVL), and are acquired using the following equations [29–31]:

$$HVL = \frac{\ln(2)}{LAC} \quad (8)$$

An absorption of 0.368 of the incident gamma radiation was observed by samples that have a thickness of one mean free path (MFP) [32]:

$$MFP = \frac{1}{LAC} \quad (9)$$

The terms of exposure buildup factor (EBF), energy absorption build-up factor (EABF) are also essential parameters to see total contributions to gamma rays' attenuation in material [33,34]. In this study, exposure build-up factor (EBF) and energy absorption build-up factor (EABF) values were also determined using G-P fitting method. The geometric progression (G-P) fitting method is often utilized to log EABFs. Following the definition of the equivalent atomic number (Z_{eq}) values, the five G-P fitting parameters for the elements (b, a, c, and d Xk) are reported from the ANS-standard database, which contains different elements with energies ranging from 0.015–15 MeV to 40 MFP. The G-P fitting parameters of the studied glasses were computed using the interpolation method. On the other hand, the term of exposure build-up factor (EBF) is the exposure in air after passing through the shielding material is the quantity of interest. The following formulas **(x,y,z)** are used to measure EABF and EBF for single-layered gamma ray shielding enclosure (GSE) with OT up to 100 MFP and energy between 0.015 and 15 MeV.

$$B(E,X) = 1 + \frac{b-1}{K-1}(K^x - 1) \; for \; K \neq 1 \quad (10)$$

$$B(E,X) = 1 + (b-1)x \; for \; K = 1 \quad (11)$$

$$K(E,x) = cx^a + \frac{d\,tanh\frac{x}{X_k - 2} - \tanh(-2)1 - \tanh(-2)}{1 - \tanh(-2)} \; for \; x \leq 40\,mfp \quad (12)$$

where E, x, and B represent the incident photon energy, penetration depth in MFP, and build-up factor at 1 MFP, respectively, and K stands for photon-dose multiplication factor [35] (see Fig. 1).

3. Results and discussion

In this study, five different glass samples encoded VPBCd0, VPBCd2, VPBCd4, VPBCd6 and VPBCd8 based on $46V_2O_5$–$46P_2O_5$–$(8-x)B_2O_3$–xCdO (x = 0–8 mol%) system were analysed in terms of their gamma-ray attenuation competencies. The experiments on optical and structural of alloys with greatly differing composition were widely published. In their research, Kilic [1] et al., have extensively investigated the impact of B_2O_3/CdO substitution on optical and structural and thermal properties of $46V_2O_5$–$46P_2O_5$–$(8-x)B_2O_3$–xCdO glasses. They found that CdO reinforcement has a major impact on structural, thermal, and optical properties semiconducting oxide glasses. Accordingly, we aimed to determine wide-range of gamma-ray attenuation properties and their numerical changes as a result of B_2O_3/CdO substitution in $46V_2O_5$–$46P_2O_5$–$(8-x)B_2O_3$–xCdO glass system. A first step was made in determination of LAC values in a 0.015–15 MeV photon energy range using general-purpose Monte Carlo code MCNPX (2.7.0) and Phy-X PSD code. The term LAC (μ) is used to assess a possible radiation shielding substance's shielding properties. This density-dependent parameter assists in determining the efficacy of shielding materials in blocking gamma rays. Fig. 2 illustrates the pattern in the linear attenuation coefficients (μ) of analysed glass samples as a function of photon energy. (i.e. between 0.015 and 15 MeV). Two distinct mechanisms exist for photons to gain energy, both of which include the use of electrons. With one case, the photon is fully absorbed; in the other, only a fraction of the light is absorbed, with the remainder dispersed. The probability that these events occur is proportional to the temperature and photon potential of the medium. The photoelectric effect appears to be greater for low-energy photons (less than 100 keV). Its probability increases dramatically as Z increases. With photons of moderate to high energy, the Compton effect is more pronounced (more than 100 keV). Only photons with an energy greater than 1.02 MeV form pairs. Considering these types of interactions, it is fair to assume that the linear attenuation coefficient is energy-dependent and varies according to these photon energy areas. Fig. 2 shows a fast decrease in energy from 0.015 MeV to 0.08 MeV. In the second region, a smooth decrement was observed, illustrating Compton scattering's superiority. Our findings suggest that the highest values were registered for the VPBCd8 study. This is demonstrated by the highest level of CdO reinforcement in the VPBCd8 sample. As shown in Table 1, the CdO reinforced VPBCd8 sample exhibits the highest glass density (3.011 g/cm^3). A review of the literature revealed that similar results have been published in which adding certain molecules with a higher atomic number increased the linear attenuation coefficients [36–39]. On the other hand, mass attenuation coefficients (MAC) are density-independent and unique to the specified material [40]. Fig. 3 shows the variance of MAC versus photon energy (E). Clearly, gamma-ray radiation energy and the chemical composition of the glasses have altered

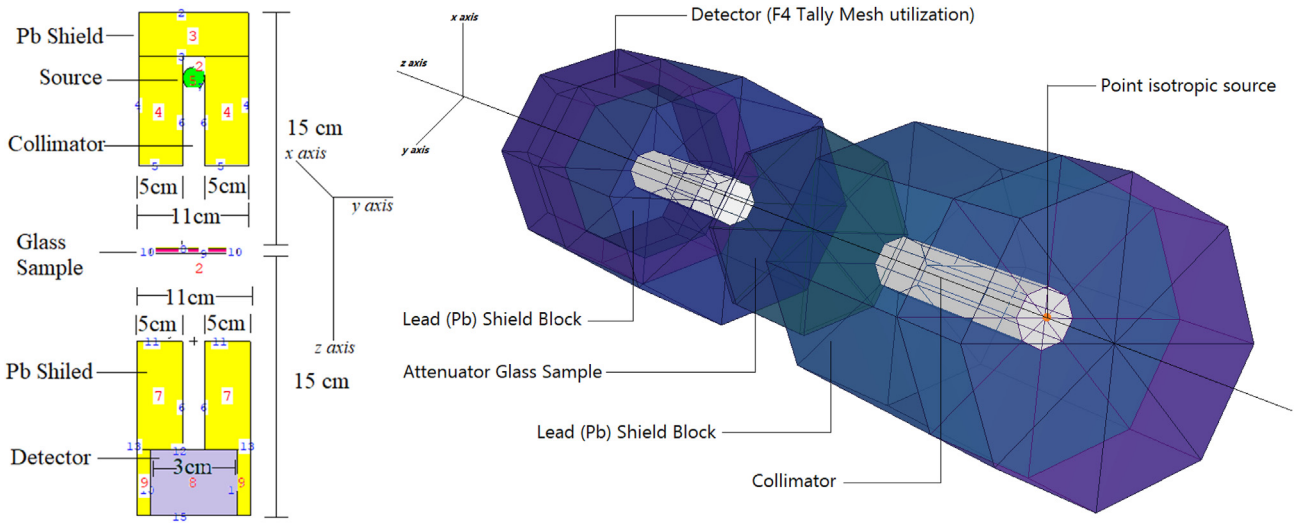

Fig. 1 – MCNPX simulation setup for gamma ray transmission studies.

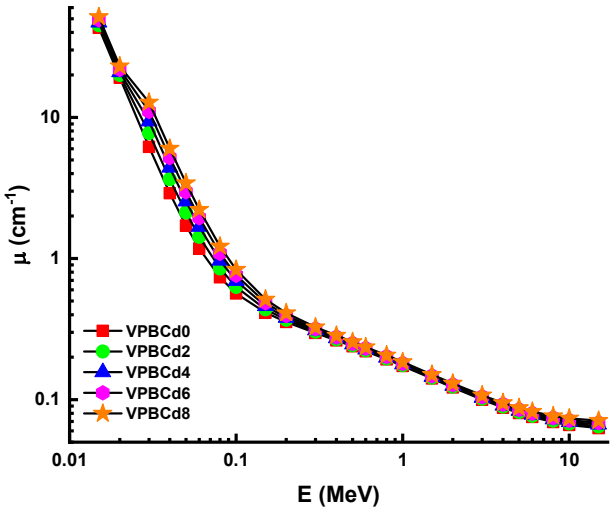

Fig. 2 – Variation of linear attenuation coefficient (μ) against Photon energy for all glasses.

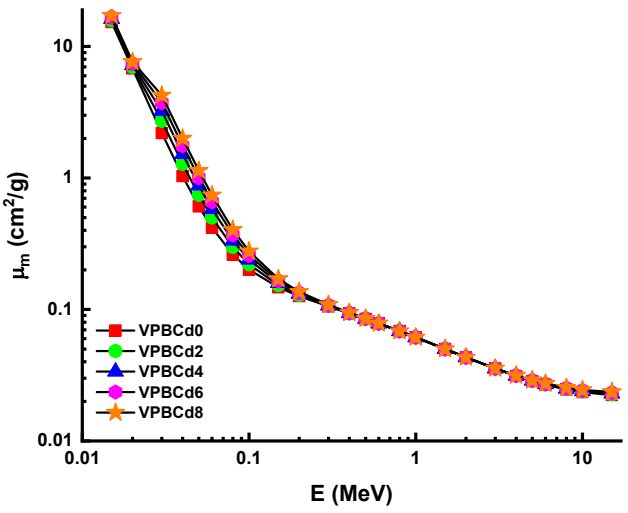

Fig. 3 – Variation of mass attenuation coefficient (μ_m) against Photon energy for all glasses.

the variation of MAC values. The MAC difference shows major patterns in three distinctive regions. In the low energy region where the photoelectric effect is a dominant process, a sharp decrease was obtained. The Compton Scattering superiority showed smooth reductions for MAC values. There are apparent higher MAC values for the VPBCd8 sample at all incident photon energies. In particular, the findings for VPBCd0, VPBCd2, VPBCd4, VPBCd6 and VPBCd8 samples were reported as 0.1471 cm^2/g, 0.1530 cm^2/g, 0.1590 cm^2/g, 0.1649 cm^2/g and 0.1707 cm^2/g at 0.15 MeV photon energy, respectively. Moreover, MAC values were reported as 0.0223 cm^2/g, 0.0226 cm^2/g, 0.0229 cm^2/g, 0.0232 cm^2/g and 0.0236 cm^2/g at 15 MeV photon energy, respectively. Our findings showed that VPBCd8 sample has the maximum MAC values among the investigated glasses. These observed behaviours in both the low and high energy regions can be explained by the higher density of VPBCd8, which includes the highest concentration of CdO additives (i.e., 8 mol%). The shielding material's gamma attenuation features should also be checked in terms of the HVL transmission factor [41,42]. Fig. 4 shows the variation of HVL values as a function of incident photon energy for all glasses. The maximum HVLs for the prepared alloys is observed at 15 MeV. However, VPBCd8 was reported with the lowest HVL values among the investigated glass samples (e.g. the best values). The HVL values were reported as 1.6756 cm, 1.5867 cm, 1.5034, 1.4257 cm and 1.3485 cm for VPBCd0, VPBCd2, VPBCd4, VPBCd6 and VPBCd8 at 0.15 MeV, respectively. In other words, 8% mole CdO reinforcement reduced the thickness of the HVL as 0.3271 cm

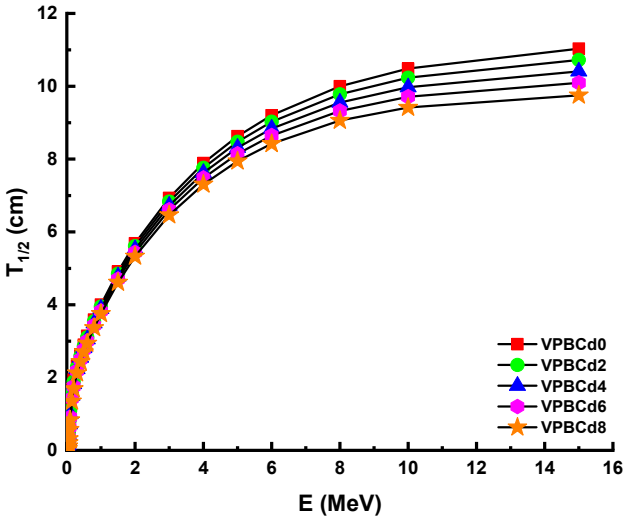

Fig. 4 – Variation of half value layer ($T_{1/2}$) against Photon energy for all glasses.

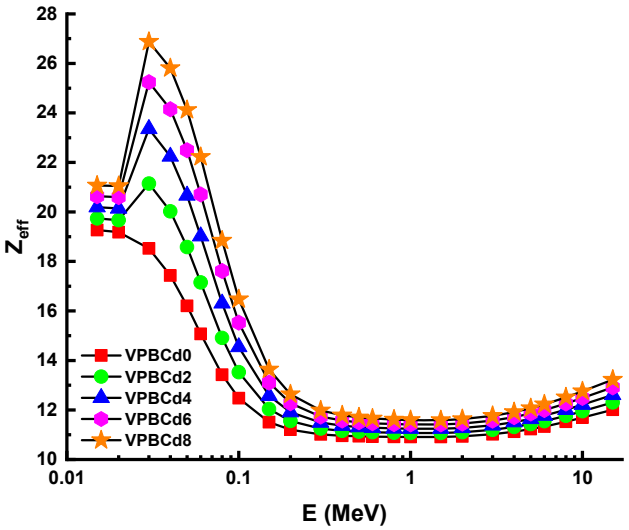

Fig. 6 – Variation of effective atomic number (Z_{eff}) against Photon energy for all glasses.

against 0.15 MeV photon energy. The finding of HVL supports the beneficial impact of CdO on increasing the gamma protection of glass samples. The term of mean free path (sometimes referred to as MFP) is also a factor in gamma-protection abilities of composite materials. The average distance traveled by photons prior to an encounter is known as MFP [40,41]. In this study, MFP values were determined for all glass samples. Fig. 5 depicts the variation of MFP values as a function of incident gamma-ray energy (MeV). The obtained behaviours of MFP values usually vary like the changing trend of HVL. Among the investigated glasses, the lowest MFP values were reported for VPBCd8 sample. This means average distance traveled by photons prior to an encounter is minimum in VPBCd8 sample, which can also be considered as another attenuation superiority against incident gamma-rays. An effective atomic number (Z_{eff}) for testing the appropriateness of the substance for gamma applications is associated with the appropriate partial photon mitigation step [42,43]. The variation of calculated Z_{eff} values of glass samples is seen in Fig. 6. Due to its superior shielding properties with the highest CdO additive, Z_{eff} values were maximum for the VPBCd8 glass sample. For example, Z_{eff} values were reported as 11.50, 12.04, 12.57, 13.11 and 13.64 for VPBCd0, VPBCd2, VPBCd4, VPBCd6 and VPBCd8 samples at 0.15 MeV, respectively. On the other hand, variation of effective electron density (N_{eff}) against Photon energy for all glasses for the five forms of glasses were determined. It can be seen from Fig. 7 that, $N_{eff\ values}$ reached to maximum at 0.03 MeV. Further, a sharp decrement trend was observed. Overall, the maximum N_{eff} values were reported for VPBCd8 sample. This is an expected result according to previous discussions on Z_{eff}. Including some secondary

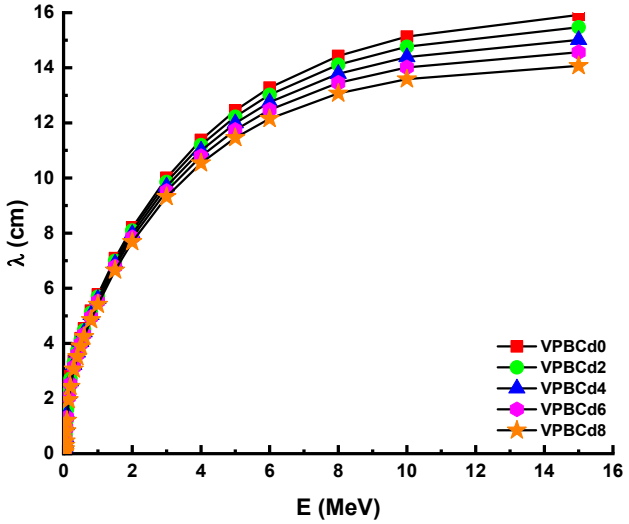

Fig. 5 – Variation of mean free path (λ) against Photon energy for all glasses.

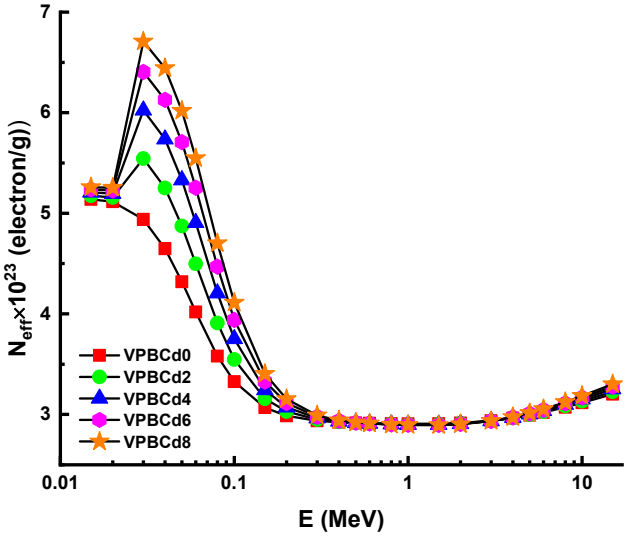

Fig. 7 – Variation of effective electron density (N_{eff}) against Photon energy for all glasses.

Table 3 – (EBF and EABF) G–P fitting coefficients (b, c, a, Xk and d) of VPBCd0 glass sample.

Energy (MeV)	Z_{eq}	G-P Fitting Parameters for EBF					G-P Fitting Parameters for EABF				
		a	b	c	d	X_k	a	b	c	d	X_k
0.015	15.82	0.306	1.017	0.311	−0.231	0.306	0.286	1.016	0.312	−0.157	11.472
0.020	16.05	0.229	1.039	0.339	−0.379	0.229	0.261	1.040	0.307	−0.503	28.668
0.030	16.29	0.221	1.110	0.380	−0.121	0.221	0.221	1.110	0.380	−0.121	13.823
0.040	16.43	0.207	1.239	0.412	−0.115	0.207	0.213	1.247	0.403	−0.122	14.662
0.050	16.54	0.183	1.404	0.472	−0.103	0.183	0.187	1.437	0.463	−0.105	14.601
0.060	16.62	0.149	1.578	0.554	−0.083	0.149	0.144	1.665	0.556	−0.079	15.298
0.080	16.72	0.088	1.880	0.723	−0.051	0.088	0.142	2.381	0.608	−0.089	13.281
0.100	16.80	0.054	2.141	0.846	−0.043	0.054	0.079	2.987	0.782	−0.063	13.476
0.150	16.91	−0.006	2.381	1.089	−0.022	−0.006	−0.006	3.705	1.091	−0.020	13.157
0.200	16.98	−0.030	2.423	1.222	−0.016	−0.030	−0.041	3.639	1.268	−0.005	15.922
0.300	17.05	−0.052	2.349	1.336	−0.010	−0.052	−0.072	3.156	1.422	0.016	18.940
0.400	17.08	−0.062	2.257	1.375	0.002	−0.062	−0.078	2.834	1.448	0.017	16.798
0.500	17.11	−0.069	2.169	1.394	0.017	−0.069	−0.079	2.608	1.447	0.020	16.443
0.600	17.12	−0.068	2.108	1.379	0.015	−0.068	−0.078	2.451	1.429	0.020	16.480
0.800	17.13	−0.065	2.009	1.346	0.017	−0.065	−0.073	2.250	1.383	0.021	15.548
1.000	17.13	−0.060	1.936	1.307	0.017	−0.060	−0.066	2.123	1.335	0.021	15.221
1.500	14.86	−0.047	1.835	1.227	0.016	−0.047	−0.049	1.943	1.235	0.017	14.907
2.000	13.94	−0.033	1.772	1.155	0.010	−0.033	−0.033	1.838	1.155	0.010	14.352
3.000	13.65	−0.010	1.670	1.058	−0.003	−0.010	−0.009	1.697	1.054	−0.003	11.290
4.000	13.58	0.007	1.594	0.996	−0.014	0.007	0.006	1.600	0.996	−0.010	12.775
5.000	13.55	0.017	1.525	0.963	−0.016	0.017	0.021	1.530	0.947	−0.024	14.420
6.000	13.53	0.022	1.477	0.944	−0.021	0.022	0.023	1.460	0.940	−0.028	15.125
8.000	13.51	0.028	1.392	0.924	−0.026	0.028	0.034	1.370	0.910	−0.029	13.016
10.000	13.49	0.037	1.333	0.905	−0.033	0.037	0.035	1.303	0.910	−0.031	13.825
15.000	13.48	0.049	1.240	0.878	−0.045	0.049	0.051	1.215	0.872	−0.048	14.254

Table 4 – (EBF and EABF) G–P fitting coefficients (b, c, a, Xk and d) of VPBCd2 glass sample.

Energy (MeV)	Z_{eq}	G-P Fitting Parameters for EBF					G-P Fitting Parameters for EABF				
		a	b	c	d	X_k	a	b	c	d	X_k
0.015	15.99	0.324	1.017	0.294	−0.251	10.453	0.301	1.016	0.295	−0.162	11.365
0.020	16.23	0.231	1.038	0.337	−0.360	26.803	0.250	1.038	0.322	−0.483	28.856
0.030	17.49	0.243	1.089	0.354	−0.142	13.556	0.243	1.089	0.354	−0.142	13.556
0.040	17.75	0.215	1.188	0.395	−0.122	14.547	0.211	1.190	0.398	−0.115	14.406
0.050	17.94	0.201	1.317	0.435	−0.114	14.241	0.208	1.341	0.422	−0.121	14.331
0.060	18.09	0.169	1.450	0.506	−0.095	14.351	0.164	1.516	0.505	−0.090	15.365
0.080	18.29	0.116	1.709	0.641	−0.066	14.369	0.178	2.090	0.524	−0.099	13.007
0.100	18.44	0.067	1.907	0.789	−0.045	14.429	0.122	2.634	0.666	−0.084	12.709
0.150	18.67	0.008	2.181	1.016	−0.022	13.604	0.027	3.458	0.958	−0.037	13.443
0.200	18.82	−0.022	2.254	1.168	−0.015	11.936	−0.016	3.541	1.149	−0.021	12.668
0.300	19.01	−0.043	2.253	1.282	−0.011	10.151	−0.048	3.188	1.309	−0.010	9.237
0.400	19.10	−0.049	2.207	1.313	−0.011	8.955	−0.066	2.841	1.386	0.014	20.770
0.500	19.16	−0.061	2.123	1.352	0.010	18.940	−0.070	2.625	1.394	0.014	17.465
0.600	19.20	−0.062	2.068	1.349	0.013	19.353	−0.071	2.460	1.390	0.017	17.294
0.800	19.23	−0.061	1.975	1.327	0.014	17.390	−0.066	2.263	1.351	0.017	16.637
1.000	19.24	−0.057	1.912	1.293	0.015	16.146	−0.061	2.128	1.311	0.017	15.703
1.500	16.26	−0.044	1.830	1.214	0.013	16.132	−0.049	1.939	1.232	0.016	14.845
2.000	14.69	−0.033	1.765	1.156	0.010	14.849	−0.033	1.837	1.155	0.010	14.041
3.000	14.20	−0.010	1.668	1.058	−0.003	11.054	−0.008	1.698	1.052	−0.004	11.521
4.000	14.10	0.002	1.586	1.010	−0.013	15.822	0.006	1.596	0.998	−0.011	12.783
5.000	14.04	0.016	1.522	0.967	−0.017	11.067	0.021	1.528	0.948	−0.026	14.617
6.000	14.01	0.019	1.474	0.953	−0.019	14.092	0.022	1.456	0.944	−0.027	15.193
8.000	13.97	0.027	1.389	0.930	−0.025	13.480	0.036	1.367	0.907	−0.031	12.006
10.000	13.95	0.036	1.331	0.908	−0.032	13.344	0.033	1.298	0.915	−0.029	13.396
15.000	13.94	0.047	1.236	0.886	−0.043	13.483	0.039	1.204	0.908	−0.037	14.303

particles in the medium, a combined radiation density correction ratio is used for the effect of scattered radiation. The concentration of secondary ionizing radiation must be addressed when calculating build-up factors. The factor of aggregation is a multiplier, which is multiplied by the reaction of the photons to determine the cumulative contribution of the photons in the attenuator environment [44]. Based on the two sub meanings of build-up factor, it can be divided into two

Table 5 – (EBF and EABF) G–P fitting coefficients (b, c, a, Xk and d) of VPBCd4 glass sample.

Energy (MeV)	Z_{eq}	G-P Fitting Parameters for EBF					G-P Fitting Parameters for EABF				
		a	b	c	d	X_k	a	b	c	d	X_k
0.015	16.17	0.308	1.016	0.311	−0.255	12.154	0.287	1.015	0.312	−0.174	12.991
0.020	16.41	0.233	1.036	0.335	−0.342	25.962	0.240	1.036	0.338	−0.464	29.040
0.030	18.54	0.232	1.073	0.366	−0.131	12.897	0.248	1.074	0.348	−0.144	12.979
0.040	18.88	0.221	1.154	0.383	−0.123	13.994	0.235	1.160	0.366	−0.142	14.571
0.050	19.12	0.216	1.264	0.408	−0.126	14.192	0.219	1.283	0.399	−0.129	14.771
0.060	19.31	0.182	1.374	0.474	−0.103	14.325	0.187	1.429	0.461	−0.106	14.791
0.080	19.58	0.137	1.597	0.588	−0.078	14.338	0.161	1.841	0.538	−0.083	14.215
0.100	19.78	0.090	1.780	0.719	−0.056	14.306	0.108	2.274	0.672	−0.074	15.108
0.150	20.09	0.025	2.055	0.945	−0.028	13.698	0.053	3.230	0.866	−0.051	13.448
0.200	20.28	−0.010	2.157	1.107	−0.020	12.615	0.006	3.440	1.057	−0.034	12.902
0.300	20.51	−0.036	2.182	1.241	−0.012	10.414	−0.037	3.159	1.250	−0.013	10.463
0.400	20.65	−0.045	2.150	1.285	−0.010	9.877	−0.056	2.845	1.333	0.014	25.340
0.500	20.74	−0.047	2.106	1.295	−0.010	8.659	−0.062	2.617	1.359	0.009	16.107
0.600	20.79	−0.056	2.042	1.320	0.011	21.354	−0.061	2.478	1.346	0.013	19.546
0.800	20.84	−0.057	1.954	1.308	0.012	17.246	−0.061	2.261	1.329	0.012	14.964
1.000	20.85	−0.055	1.894	1.283	0.016	17.498	−0.057	2.129	1.296	0.016	16.660
1.500	17.53	−0.043	1.818	1.212	0.013	16.234	−0.047	1.942	1.225	0.015	15.012
2.000	15.43	−0.032	1.762	1.153	0.009	15.062	−0.032	1.838	1.151	0.009	14.732
3.000	14.76	−0.010	1.665	1.059	−0.003	12.710	−0.009	1.694	1.055	−0.004	11.365
4.000	14.61	0.004	1.588	1.006	−0.014	15.380	0.007	1.596	0.996	−0.013	12.695
5.000	14.53	0.016	1.521	0.968	−0.017	11.550	0.022	1.526	0.948	−0.027	14.571
6.000	14.49	0.019	1.472	0.955	−0.019	14.194	0.022	1.454	0.945	−0.028	15.388
8.000	14.44	0.028	1.389	0.929	−0.026	13.560	0.036	1.364	0.909	−0.031	11.855
10.000	14.42	0.037	1.331	0.908	−0.033	13.352	0.036	1.298	0.910	−0.032	13.498
15.000	14.40	0.049	1.236	0.884	−0.046	13.256	0.035	1.198	0.920	−0.035	14.383

Table 6 – (EBF and EABF) G–P fitting coefficients (b, c, a, Xk and d) of VPBCd6 glass sample.

Energy (MeV)	Z_{eq}	G-P Fitting Parameters for EBF					G-P Fitting Parameters for EABF				
		a	b	c	d	X_k	a	b	c	d	X_k
0.015	16.35	0.292	1.016	0.330	−0.258	13.876	0.273	1.015	0.330	−0.185	14.629
0.020	16.58	0.235	1.035	0.333	−0.325	25.162	0.230	1.035	0.352	−0.445	29.215
0.030	19.47	0.220	1.062	0.378	−0.116	12.005	0.241	1.063	0.357	−0.142	12.689
0.040	19.87	0.232	1.132	0.366	−0.134	14.050	0.224	1.131	0.378	−0.124	13.940
0.050	20.15	0.214	1.222	0.404	−0.118	14.136	0.226	1.236	0.388	−0.133	14.225
0.060	20.37	0.193	1.322	0.452	−0.111	14.244	0.193	1.367	0.445	−0.108	14.765
0.080	20.69	0.147	1.525	0.560	−0.082	14.367	0.143	1.689	0.556	−0.078	15.754
0.100	20.92	0.102	1.696	0.682	−0.062	14.267	0.113	2.099	0.650	−0.074	15.803
0.150	21.28	0.037	1.967	0.900	−0.033	13.792	0.075	3.050	0.803	−0.066	13.792
0.200	21.51	0.001	2.082	1.061	−0.023	12.760	0.024	3.309	0.993	−0.043	12.954
0.300	21.78	−0.029	2.129	1.204	−0.014	10.779	−0.025	3.128	1.195	−0.019	10.971
0.400	21.94	−0.040	2.108	1.259	−0.011	10.099	−0.047	2.839	1.288	0.005	21.738
0.500	22.04	−0.045	2.068	1.280	−0.010	8.573	−0.055	2.619	1.323	0.003	14.542
0.600	22.10	−0.052	2.016	1.300	0.006	17.751	−0.055	2.480	1.317	0.006	17.003
0.800	22.16	−0.051	1.941	1.287	0.006	14.664	−0.055	2.265	1.305	0.005	13.120
1.000	22.17	−0.053	1.879	1.274	0.015	18.052	−0.055	2.129	1.285	0.015	17.144
1.500	18.70	−0.044	1.807	1.213	0.013	15.554	−0.046	1.940	1.222	0.014	14.971
2.000	16.15	−0.031	1.760	1.149	0.008	15.178	−0.030	1.839	1.147	0.007	15.767
3.000	15.31	−0.010	1.663	1.059	−0.004	12.398	−0.009	1.692	1.057	−0.003	11.482
4.000	15.11	0.006	1.590	1.002	−0.016	14.495	0.008	1.595	0.994	−0.014	12.683
5.000	15.02	0.016	1.521	0.968	−0.018	11.996	0.022	1.524	0.948	−0.028	14.533
6.000	14.96	0.018	1.470	0.958	−0.019	14.291	0.022	1.452	0.946	−0.029	15.574
8.000	14.90	0.029	1.389	0.928	−0.028	13.651	0.036	1.362	0.911	−0.031	11.760
10.000	14.87	0.038	1.330	0.907	−0.035	13.342	0.038	1.298	0.905	−0.035	13.656
15.000	14.85	0.052	1.235	0.880	−0.050	13.108	0.034	1.194	0.928	−0.034	14.464

Table 7 – (EBF and EABF) G–P fitting coefficients (b, c, a, Xk and d) of VPBCd8 glass sample.

Energy (MeV)	Z_{eq}	G-P Fitting Parameters for EBF					G-P Fitting Parameters for EABF				
		a	b	c	d	X_k	a	b	c	d	X_k
0.015	16.51	0.276	1.015	0.347	−0.261	15.521	0.259	1.014	0.348	−0.196	16.194
0.020	16.75	0.237	1.034	0.331	−0.309	24.398	0.220	1.033	0.366	−0.428	29.382
0.030	20.30	0.224	1.055	0.372	−0.130	12.538	0.238	1.054	0.360	−0.148	13.147
0.040	20.75	0.236	1.119	0.360	−0.133	13.730	0.226	1.117	0.373	−0.123	13.853
0.050	21.06	0.217	1.201	0.397	−0.121	14.114	0.229	1.213	0.380	−0.133	14.256
0.060	21.31	0.196	1.290	0.444	−0.112	14.231	0.199	1.330	0.431	−0.113	14.753
0.080	21.67	0.154	1.473	0.542	−0.085	14.390	0.153	1.619	0.533	−0.084	15.624
0.100	21.92	0.111	1.631	0.655	−0.065	14.234	0.127	1.993	0.615	−0.081	15.631
0.150	22.32	0.047	1.894	0.863	−0.036	13.870	0.093	2.901	0.751	−0.079	14.077
0.200	22.57	0.009	2.020	1.023	−0.026	12.879	0.038	3.202	0.941	−0.050	12.996
0.300	22.87	−0.024	2.086	1.174	−0.015	11.077	−0.015	3.102	1.151	−0.023	11.384
0.400	23.05	−0.036	2.075	1.238	−0.012	10.279	−0.039	2.834	1.252	−0.003	18.828
0.500	23.15	−0.043	2.038	1.268	−0.009	8.504	−0.049	2.621	1.294	−0.002	13.287
0.600	23.22	−0.048	1.995	1.284	0.001	14.857	−0.050	2.482	1.294	0.001	14.960
0.800	23.28	−0.047	1.930	1.270	0.001	12.581	−0.050	2.269	1.285	0.000	11.632
1.000	23.30	−0.051	1.867	1.266	0.015	18.499	−0.053	2.130	1.276	0.014	17.535
1.500	19.80	−0.043	1.798	1.211	0.013	15.668	−0.046	1.937	1.222	0.015	15.466
2.000	16.85	−0.031	1.756	1.148	0.007	15.171	−0.031	1.836	1.149	0.008	15.710
3.000	15.84	−0.009	1.661	1.059	−0.005	10.698	−0.010	1.691	1.059	−0.002	11.791
4.000	15.61	0.008	1.588	0.998	−0.017	12.053	0.007	1.593	0.996	−0.013	12.914
5.000	15.50	0.014	1.518	0.974	−0.017	12.134	0.020	1.518	0.955	−0.027	14.597
6.000	15.43	0.019	1.469	0.958	−0.021	13.929	0.022	1.448	0.949	−0.029	15.400
8.000	15.36	0.030	1.389	0.928	−0.029	13.581	0.033	1.357	0.918	−0.029	12.240
10.000	15.33	0.037	1.328	0.911	−0.034	13.467	0.039	1.296	0.905	−0.036	13.610
15.000	15.30	0.051	1.233	0.885	−0.050	13.116	0.035	1.192	0.928	−0.035	14.412

types: Exposure Build-up Factor (EBF) and Energy Absorption Build-up Factor. (EABF). In our study, EBF and EABF values of five different glasses were calculated using a G-P fit method between 0.5 and 40 MFP and listed in Tables 3–7. Fig. 8 (a–e) and Fig. 9 (a–e) shows the variation of exposure build-up factor (EBF) and energy absorption build-up factor against photon energy for all glasses. Fig. 8 (a–e) indicates that different penetration depths up to 40 MFP are comprised of three distinct regions of EBF versus photon radiation. Regions which interact with photons are central to the fundamental interactions between photons and matter. Since photoelectric influence is negligible near the high atomic numbers' binding energy, the first area showed peaks. On the other hand. the third area of the sample is of interest to pair development where, due to absorption processes, the EBF values decrease. Moreover, some numerical highlights were presented in Fig. 8 (a–e). The overall results showed that minimum EBF values were reported for VPBCd8 sample at all MFP values. This situation clearly indicates that superiority of VPBCd8 is confirmed with exposure build-up factor values as well. The similar trend was also reported for energy absorption build-up factor (EABF) values. The minimal values of EABF were reported for VPBCd8 sample at all MFP values. An extensive comparison was made in terms of EBF and EABF values depending on glass composition at certain MFP values such as 10, 20, 30 and 40 MFP. Figs. 10 and 11 shows the variation of exposure build-up factor (EBF) energy absorption build-up factor (EABF) against glass compositions at 0.4 MeV photon energy. Among the investigated MFP values, the minimum EBF and EABF values were reported at 10 MFP. However, a sharp decrement in EBF and EABF vales was reported from 0 to 8 mol % at 40 MFP. On the other hand, a smooth decrement in EBF and EABF vales was reported from 0 to 8 mol % at 10 MFP. This situation can be explained by attenuation process of gamma ray photons in different depths depending on attenuation properties of shielding material. Fig. 12 indicates the difference in the rate of energy absorption build-up factor (EABF) and exposure build-up factor (EBF) for all glasses versus atomic number (Z_{eff}). It can be clearly seen from Fig. 12 that there is a strict dependence between effective atomic numbers an EBF-EABF values. Almost a linear decrement was observed from 0 to 8 mol %.

4. Conclusion

This study aimed to determine the contribution of B_2O_3/CdO substitution on gamma-ray attenuation behaviors of $46V_2O_5–46P_2O_5–(8\text{-}x)B_2O_3–xCdO$ (x = 0–8 mol%) glass system. The result showed that B_2O_3/CdO substitution has a direct effect on behaviors of studied semiconducting oxide glasses against ionizing gamma-rays. Our findings showed that increasing CdO reinforcement has an obvious impact on gamma-ray attenuation properties especially in the low energy range, where photoelectric effect dominates the photon–matter interaction. Moreover, half-value layer, mean-free path and tenth value layer also decrease with an increase in the content of CdO in the composition. Consequently, VPBCd8 sample with 8% mole CdO additive was reported with the minimum half-value layer, the mean-free path, tenth value layer exposure build-up factor and energy absorption build-up factors. The outcomes of our investigation have revealed the following bullet points;

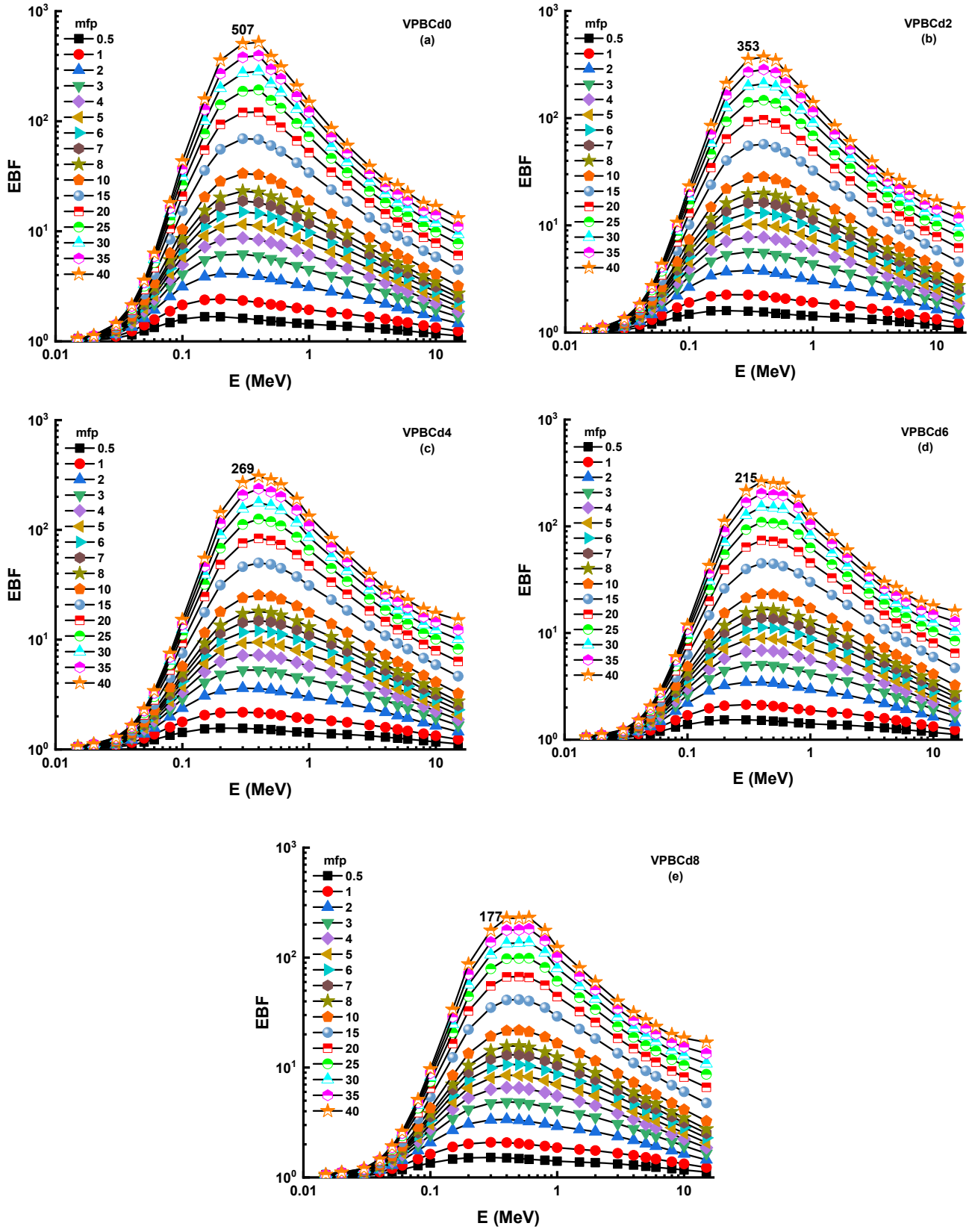

Fig. 8 – (a–e) Variation of exposure buildup factor (EBF) against Photon energy for all glasses.

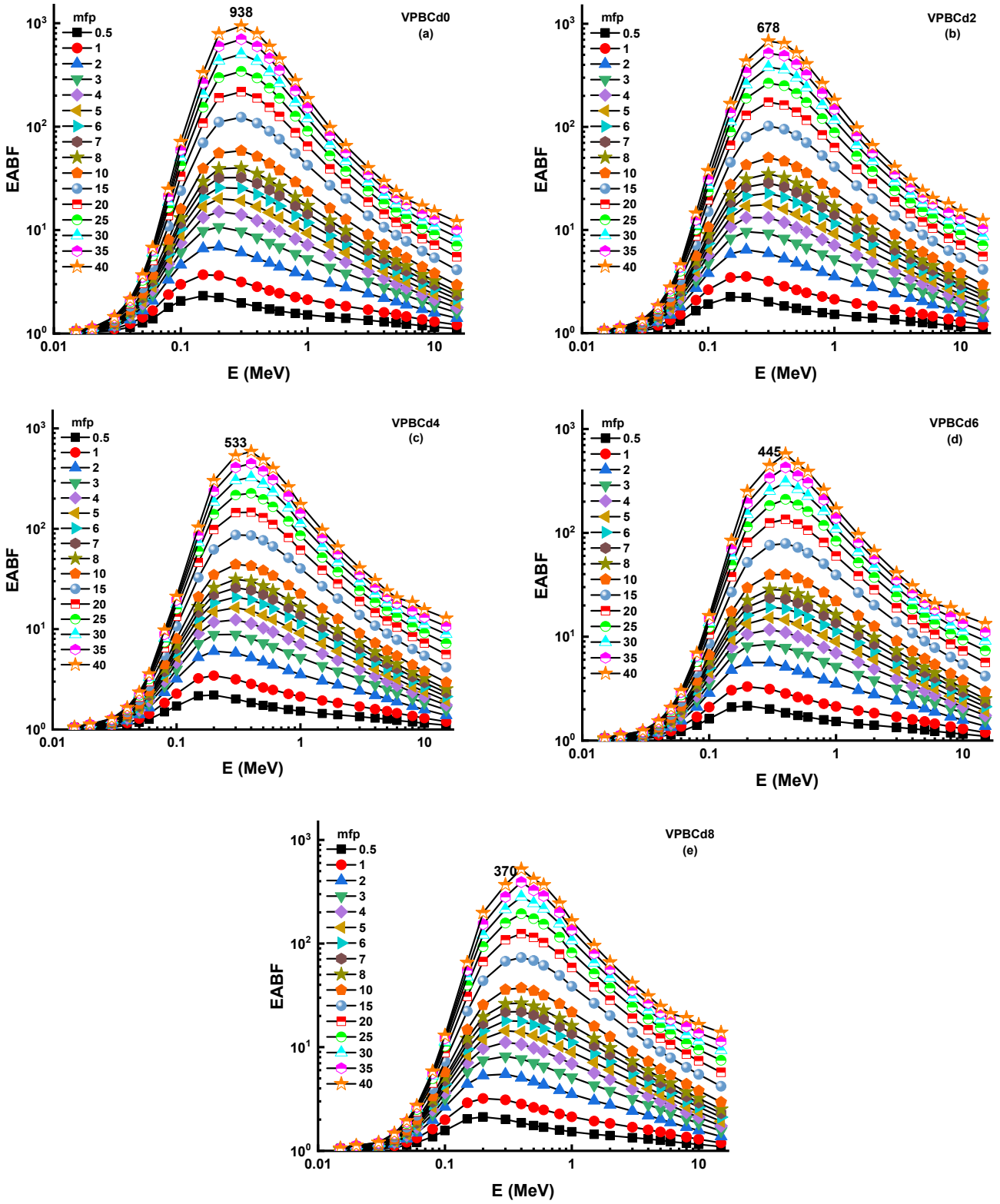

Fig. 9 – (a–e) Variation of energy absorption buildup factor (EABF) against Photon energy for all glasses.

i) The MAC values of 0.1471 cm^2/g, 0.1530 cm^2/g, 0.1590 cm^2/g, 0.1649 cm^2/g, 0.1707 were reported for VPBCd0, VPBCd2, VPBCd4, VPBCd6, VPBCd8 at 0.15 MeV, respectively. Generally, MAC values were ordered in the trend of: $(MAC)_{VPBCd8} > (MAC)_{VPBCd6} > (MAC)_{VPBCd4} > (MAC)_{VPBCd2} > (MAC)_{VPBCd0}$

ii) The HVL values of 1.676 cm, 1.587 cm, 1.503 cm, 1.426 cm, 1.348 were recorded VPBCd0, VPBCd2, VPBCd4, VPBCd6, VPBCd8 at 0.15 MeV, respectively. HVL

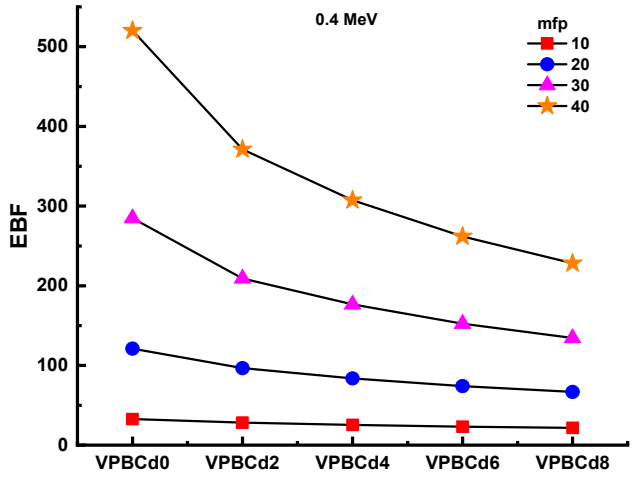

Fig. 10 – Variation of exposure buildup factor (EBF) against glass compositions.

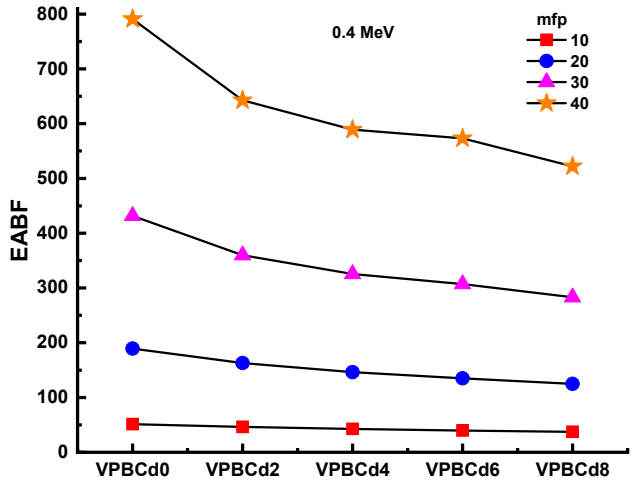

Fig. 11 – Variation of energy absorption buildup factor (EABF) against glass compositions.

values were ordered in the trend of $(HVL)_{VPBCd8} < (HVL)_{VPBCd6} < (HVL)_{VPBCd4} < (HVL)_{VPBCd2} < (HVL)_{VPBCd0}$

iii) Our findings indicated that VPBCd8 had the lowest mean free path and EBF/EABF values in addition to highest the highest Z_{eff} values values at all photon energies.

A future study that can be recommended based on the results is the variation of CdO ratio in the glass composition. In this study, we could reach until 8% of CdO additive in $46V_2O_5–46P_2O_5–(8–x)B_2O_3–xCdO$ glass system. Accordingly, our findings showed that increasing CdO reinforcement has an obvious impact on gamma-ray attenuation properties. To increase the obtained shielding properties with increasing CdO, a direct molar increase may continue up to a certain value (i.e., above 8% mole CdO). However, it is worth

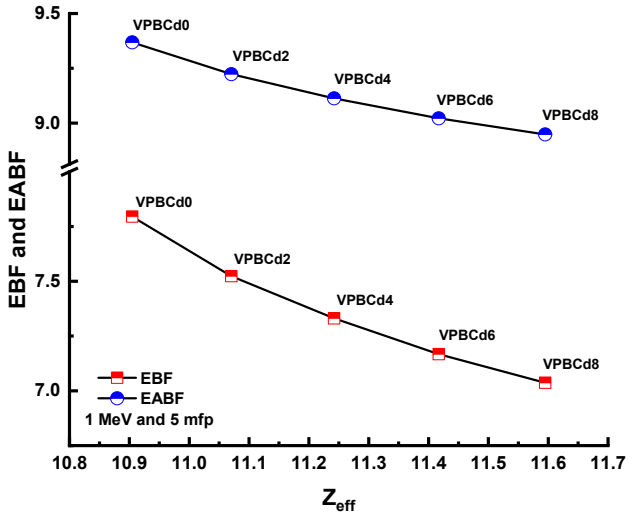

Fig. 12 – Variation of energy absorption buildup factor (EABF) and exposure buildup factor (EBF) against effective atomic number (Z_{eff}) for all glasses.

mentioning that after a certain value, it may lose its glassy structure and show crystallization. This situation might affect the consistency of glass synthesis process. Hereby, a future study can be underlined with higher amounts of CdO reinforcement in 46V2O5–46P2O5–(8–x)B2O3–xCdO system for better shielding properties. However, it should be ensured that this increase rate does not damage the glassy structure. The outcomes would be useful for scientific community to observe the most suitable substitution type along with related semiconducting oxide glass composition to provide the shielding properties in terms of needs and utilization requirements.

Declaration of Competing Interest

The authors declare that there is no conflict of interests regarding the publication of this paper.

Acknowledgement

The authors thank Taif University Researchers Supporting Project number (TURSP-2020/12), Taif University, Taif, Saudi Arabia.

REFERENCES

[1] Kilic G, Ilik E, Issever UG, Peker M. The effect of B_2O_3/CdO substitution on structural, thermal, and optical properties of new black PVB/Cd semiconducting oxide glasses. Appl Phys A Mater Sci Process 2020;126:507. https://doi.org/10.1007/s00339-020-03689-x.

[2] Rashad M, Saudi HA, Zakaly HMH, Issa SAM, Abd-Elnaiem AM. Control optical characterizations of Ta+5–doped B_2O_3–Si_2O–CaO–BaO glasses by irradiation dose. Opt Mater (Amst) 2021;112:110613. https://doi.org/10.1016/j.optmat.2020.110613.

[3] Abdel-Khalek EK, Mohamed EA, Salem SM, Kashif I. Structural and dielectric properties of (100−x)B_2O_3-(x/2)Bi_2O_3–(x/2)Fe_2O_3 glasses and glass-ceramic containing $BiFeO_3$ phase. J Non-Cryst Solids 2018;492:41–9. https://doi.org/10.1016/j.jnoncrysol.2018.04.020.

[4] Mostafa AMA, Zakaly HM, Al-Ghamdi SA, Issa SA, Al-Zaibani M, Ramadan RM, et al. PbO–Sb_2O_3–B_2O_3–CuO glassy system: evaluation of optical, gamma and neutron shielding properties. Mater Chem Phys 2021;258. https://doi.org/10.1016/j.matchemphys.2020.123937.

[5] Saddeek YB, Aly KA, Shaaban KS, Ali AM, Alqhtani MM, Alshehri AM, et al. Physical properties of B_2O_3–TeO_2–Bi_2O_3 glass system. J Non-Cryst Solids 2018;498:82–8. https://doi.org/10.1016/j.jnoncrysol.2018.06.002.

[6] Tuscharoen S, Kaewkhao J, Limkitjaroenporn P, Limsuwan P, Chewpraditkul W. Improvement of BaO:B_2O_3:Fly ash glasses: radiation shielding, physical and optical properties. Ann Nucl Energy 2012;49:109–13. https://doi.org/10.1016/j.anucene.2012.05.017.

[7] Montani RA, Frechero MA. Mixed ion-polaron transport in lithium vanadium–molybdenum tellurite glasses. Solid State Ionics 2006;177(33–34):2911–5. https://doi.org/10.1016/j.ssi.2006.08.015.

[8] Saddeek YB, Shaaban ER, Aly KA, Sayed IM. Crystallization kinetics of Li_2O–PbO–V_2O_5 glasses. Phys B Condens Matter 2009;404(16):2412–8. https://doi.org/10.1016/j.physb.2009.04.051.

[9] Issever UG, Kilic G, Ilik E. The impact of CuO on physical, structural, optical and thermal properties of dark VPB semiconducting glasses. Opt Mater 2021;116:111084. https://doi.org/10.1016/j.optmat.2021.111084.

[10] Ilik E, Kilic G, Issever UG. Synthesis of novel AgO-doped vanadium–borophosphate semiconducting glasses and investigation of their optical, structural, and thermal properties. J Mater Sci Mater Electron 2020;31:8986–95. https://doi.org/10.1007/s10854-020-03432-5.

[11] Barde RV, Waghuley SA. Transport and physical properties of V2O5–P2O5–B2O3 glasses doped with Dy2O3. J Adv Ceram 2013;2:246–51. https://doi.org/10.1007/s40145-013-0067-8.

[12] Tekin HO, Altunsoy EE, Kavaz E, Sayyed MI, Agar O, Kamislioglu M. Photon and neutron shielding performance of boron phosphate glasses for diagnostic radiology facilities. Results Phys 2019;12:1457–64. https://doi.org/10.1016/j.rinp.2019.01.060.

[13] Chen Z, Zhang Z, Xie J, Guo Q, Yu T, Zhao P, et al. Multi-objective optimization strategies for radiation shielding design with genetic algorithm. Comput Phys Commun 2020:107267. https://doi.org/10.1016/j.cpc.2020.107267.

[14] Poltabtim W, Wimolmala E, Saenboonruang K. Properties of lead-free gamma-ray shielding materials from metal oxide/EPDM rubber composites. Radiat Phys Chem 2018;153:1–9. https://doi.org/10.1016/j.radphyschem.2018.08.036.

[15] Al-Hadeethi Y, Tijani SA. The use of lead-free transparent 50BaO-(50-x)borosilicate-xBi_2O_3 glass system as radiation shields in nuclear medicine. J Alloys Compd 2019;803:625–30. https://doi.org/10.1016/j.jallcom.2019.06.259.

[16] Elazaka AI, Zakaly HMH, Issa SAM, Rashad M, Tekin HO, Saudi HA, et al. New approach to removal of hazardous Bypass Cement Dust (BCD) from the environment: 20Na_2O-20BaC_{l2}-(60-x)B_2O_3-(x)BCD glass system and Optical, mechanical, structural and nuclear radiation shielding competences. J Hazard Mater 2021:403. https://doi.org/10.1016/j.jhazmat.2020.123738.

[17] Sallam OI, Alhodaib A, Abd El Aal S, Ezz-Eldin FM. Influence of gamma ray on optical and structural properties of commercial glass enriched with copper oxide. Inorg Chem Commun 2021;124:108388. https://doi.org/10.1016/j.inoche.2020.108388.

[18] Saudi HA, Abd-Allah WM, Shaaban KS. Investigation of gamma and neutron shielding parameters for borosilicate glasses doped europium oxide for the immobilization of radioactive waste. J Mater Sci Mater Electron 2020;31:6963–76. https://doi.org/10.1007/s10854-020-03261-6.

[19] Zakaly HM, Abouhaswa AS, Issa SAM, Mostafa MYA, Pyshkina M, El-Mallawany R. Optical and nuclear radiation shielding properties of zinc borate glasses doped with lanthanum oxide. J Non-Cryst Solids 2020;543:120151. https://doi.org/10.1016/j.jnoncrysol.2020.120151.

[20] Abouhaswa AS, Perişanoğlu U, Tekin HO, Kavaz E, Henaish AMA. Nuclear shielding properties of B_2O_3–Pb_3O_4–ZnO glasses: multiple impacts of Er_2O_3 additive. Ceram Int 2020;46:27849–59. https://doi.org/10.1016/j.ceramint.2020.07.283.

[21] Şakar E, Özpolat ÖF, Alım B, Sayyed MI, Kurudirek M. Phy-X/PSD: development of a user friendly online software for calculation of parameters relevant to radiation shielding and dosimetry. Radiat Phys Chem 2020;166:108496. https://doi.org/10.1016/j.radphyschem.2019.108496.

[22] RSICC Computer Code Collection. MCNPX user's manual version 2.4.0. MonteCarlo N-particle transport code system for multiple and high energy applications. 2002.

[23] Zakaly HMH, Saudi HA, Issa SAM, Rashad M, Elazaka AI, Tekin HO, et al. Alteration of optical, structural, mechanical durability and nuclear radiation attenuation properties of barium borosilicate glasses through BaO reinforcement: experimental and numerical analyses. Ceram Int 2020;47(4):5587–96. https://doi.org/10.1016/j.ceramint.2020.10.143.

[24] Kaur P, Singh D, Singh T. Heavy metal oxide glasses as gamma rays shielding material. Nucl Eng Des 2016;307:364–76. https://doi.org/10.1016/j.nucengdes.2016.07.029.

[25] Tekin HO, Sayyed MI, Issa SAM. Gamma radiation shielding properties of the hematite-serpentine concrete blended with WO_3 and Bi_2O_3 micro and nano particles using MCNPX code. Radiat Phys Chem 2018;150:95–100.

[26] Tekin HO, Singh VP, Manici T. Effects of micro-sized and nano-sized WO_3 on mass attenauation coefficients of concrete by using MCNPX code. Appl Radiat Isot 2017;121:122–5. https://doi.org/10.1016/j.apradiso.2016.12.040.

[27] Mostafa AMA, Zakaly HMH, Pyshkina M, Issa SAM, Tekin HO, Sidek HAA, et al. Multi-objective optimization strategies for radiation shielding performance of BZBB glasses using Bi_2O_3: a FLUKA Monte Carlo code calculations. J Mater Res Technol 2020;9:12335–45. https://doi.org/10.1016/j.jmrt.2020.08.077.

[28] Tekin HO, Issa SAM, Kavaz E, Altunsoy Guclu EE. The direct effect of Er_2O_3 on bismuth barium telluro borate glasses for nuclear security applications. Mater Res Express 2019;6:115212. https://doi.org/10.1088/2053-1591/ab4cb5.

[29] Al-Buriahi MS, Tekin HO, Kavaz E, Tonguc BT, Rammah YS. New transparent rare earth glasses for radiation protection applications. Appl Phys A Mater Sci Process 2019;125:866. https://doi.org/10.1007/s00339-019-3077-8.

[30] Mostafa AMA, Issa SAM, Zakaly HMH, Zaid MHM, Tekin HO, Matori KA, et al. The influence of heavy elements on the ionizing radiation shielding efficiency and elastic properties of some tellurite glasses: theoretical investigation. Results Phys 2020;19:103496. https://doi.org/10.1016/j.rinp.2020.103496.

[31] Rashad M, Tekin HO, Zakaly HM, Pyshkina M, Issa SAM, Susoy G. Physical and nuclear shielding properties of newly synthesized magnesium oxide and zinc oxide nanoparticles. Nucl Eng Technol 2020;52:2078–84. https://doi.org/10.1016/j.net.2020.02.013.

[32] Lakshminarayana G, Elmahroug Y, Kumar A, Tekin HO, Rekik N, Dong M, et al. Detailed inspection of γ-Ray, fast and thermal neutrons shielding competence of calcium oxide or strontium oxide comprising bismuth borate glasses. Materials 2021;14:2265. https://doi.org/10.3390/ma14092265.

[33] Issa SAM, Tekin HO, Erguzel TT, Susoy G. The effective contribution of PbO on nuclear shielding properties of xPbO-(100−x)P_2O_5 glass system: a broad range investigation. Appl Phys A 2019;125:640. https://doi.org/10.1007/s00339-019-2941-x.

[34] Al-Buriahi MS, Mann KS. Radiation shielding investigations for selected tellurite-based glasses belonging to the TNW system. Mater Res Express 2019;6:105206. https://doi.org/10.1088/2053-1591/ab3f85.

[35] Singh VP, Badiger NM. A Comprehensive study on gamma-ray exposure build-up factors and fast neutron removal cross sections of fly-ash bricks. J Ceram 2013;2013:13. https://doi.org/10.1155/2013/967264. Article ID 967264.

[36] Tekin HO, Alomairy S, Al-Buriahi MS, Rammah Y. Linear/nonlinear optical parameters along with photon attenuation effectiveness of Dy^{3+} ions doped zinc-aluminoborosilicate glasses. Phys Scripta 2021;96:065704. https://doi.org/10.1088/1402-4896/abf452.

[37] Kilic G, Ilik E, Issa SAM, Issa B, Al-Buriahi MS, Issever UG, et al. Ytterbium (III) oxide reinforced novel TeO_2-B_2O_3-V_2O_5 glass system: synthesis and optical, structural, physical and thermal properties. Available online 19 Ceram Int March 2021;47(13):18517–31. https://doi.org/10.1016/j.ceramint.2021.03.175.

[38] Rammah YS, Abouhaswa AS, Sayyed MI, Tekin HO, El-Mallawany R. Structural, UV and shielding properties of ZBPC glasses. J Non-Cryst Solids 2019;509:99–105. https://doi.org/10.1016/j.jnoncrysol.2018.12.013.

[39] Mahmoud IS, Issa SAM, Saddek YB, Tekin HO, Kilicoglu O, Alharbi T, et al. Gamma, neutron shielding and mechanical parameters for vanadium lead vanadate glasses. Ceram Int 2019;45:14058–72. https://doi.org/10.1016/j.ceramint.2019.04.105.

[40] Issa Shams AM, Tekin HO. The multiple characterization of gamma, neutron and proton shielding performances of xPbO-(99-x)B_2O_3–Sm_2O_3 glass system. Ceram Int 2019;45:23561–71. https://doi.org/10.1016/j.ceramint.2019.08.065.

[41] Al-Buriahi MS, Tonguc BT. Study on gamma-ray buildup factors of bismuth borate glasses. Appl Phys A 2019;125:482. https://doi.org/10.1007/s00339-019-2777-4.

[42] Abouhaswa AS, Mhareb MHA, Alalawi A, Al-Buriahi MS. Physical, structural, optical, and radiation shielding properties of B_2O_3-20Bi_2O_3-20Na_2O-Sb_2O_3 glasses: role of Sb_2O_3. J Non-Cryst Solids 2020;543:120130. https://doi.org/10.1016/j.jnoncrysol.2020.120130.